

The Study on The Cooling of The Hot Side of The Thermoelectric Modules Utilized For High Cooling Requirements*

Anıl Başaran^{1*} , Uğur Pehlivanoglu² 

¹ Manisa Celal Bayar Üniversitesi, Makine Mühendisliği Bölümü Manisa, Türkiye

² ISM Makine Elektrik Sanayi ve Ticaret A.Ş. Tasarım Merkezi

* anil.basaran@cbu.edu.tr

*Orcid: 0000-0003-0651-1453

Received: 19 March 2021

Accepted: 24 June 2021

DOI: 10.18466/cbayarfbe.899975

Abstract

Thermoelectric modules (TEM) without moving parts are systems that can create a cooling effect in a short time, operate quietly and most importantly do not require working fluids for cooling. In the current study, TEM selection and design were made for 300 W cooling requirement. It is known that the cooling effects of the thermoelectric modules are directly proportional to the effective cooling of the hot side of the thermoelectric module. In this respect, air and water cooler for the hot side were investigated to provide maximum COP values via effective cooling of the hot side of the TEMs. The heat sinks and fan combinations were analyzed and optimized to cool the hot side of the TEM. Different fan speeds, heat sink geometries, and heat sink locations were discussed to cool the hot side. Heat sink dimensions were optimized for specific air velocity and the thermal resistance of the thermal paste was also considered. In addition to the heat sinks and fan combinations, the water-cooling systems were investigated for the cooling of the hot side of the TEMs. Considering the thermal paste effects and leakage risk in the designs, direct-contact and non-contact water-cooled designs have been realized. In the non-contact design, the effects of aluminum and copper materials on heat transfer were discussed in addition to the impact of geometry. It was found that air-cooled systems give rise to higher temperatures at the hot side of the TEM than water cooling system. Therefore, it is concluded that water cooling systems are more effective solutions for high-capacity TEMs cooling applications.

Keywords: Thermoelectric module, Numerical simulation, Peltier module, TEM air cooling, TEM water cooling.

1. Introduction

Thermoelectric modules (TEMs) are systems that can create refrigeration by taking advantage of the Peltier effect. For this reason, TEMs are commonly defined as "Peltier modules" in the industry. TEMs are formed by the serial connection of P type semiconductors with low energy level and N type semiconductors with high energy level. Thanks to these semiconductors, TEMs can transfer heat by using the energy levels of electrons. The current passing through the P and N type semiconductors carries the energy from the cold surface to the hot surface. In other words, when current is passed through the thermoelectric element, the Peltier effect occurs and while one side of the module is cooling, the other side heats up [1].

Studies on the cooling effect of TEMs are available in the literature. Riffat et al. [2] investigated the

performance of thermoelectric cooling systems with two different configurations. In the first configuration, the authors placed the finned surface on the cold side of the thermoelectric element, while in the second configuration, they placed phase change material. A finned heat pipe was used to cool the hot side of TEM in both configurations. With their study, the author concluded that the use of phase-change materials increases the cooling performance of the thermoelectric element.

Venkatesan and Venkataramanan [3] conducted experimental and simulation studies focus on developing performance specifications on a typical thermoelectric cooler. Their study involve voltage, current and cooling capacity for various hot side temperature range of the TEM. The authors simulated the TEM performance via CFD techniques for the TEM hot side temperature ranges of 303.15-333.15 K.

Ahiska and Ahiska [4] conducted a study on the capabilities of the thermoelectric module for cooling the computer processor. In their work, they discussed two- and single-phase fluid flow as well as fan-air combination as cooling options for the hot side of TEM. They found that the two-phase system had about five times more cooling effect than the air-cooling system.

Deniz et al. [5] performed an experimental study on the performance of TEMs connected in series. They discussed air and water-cooling systems for voltage values of TEMs in the range of 5 to 15 V. In their study, it is observed that the coefficient of performance (COP) obtained in the air-cooled system was higher than the water-cooled system. Besides, as a result of their experiments, it is found that high COP values obtained at low voltage values in both systems.

Jeong [6] carried out a theoretical investigation to optimize TEMs. The author proposed a novel one-dimensional analytic model. The model is used to determine optimum current, which maximizes the COP, by using the cooling capacity, the hot and cold side temperatures, the thermal and electrical contact resistances and the properties of thermoelectric material, but not by the length of a thermoelement.

Jeong [7] also conducted a theoretical investigation to optimize thermoelectric modules for maximization of cooling capacity. The author proposed a novel one-dimensional analytic model, in which the thermal resistances of heat exchangers as well as the thermal and electrical contact resistances inherent in the modules are taken into account. In the study, it was showed the effects of thermal resistances and the contact resistances on maximum cooling capacity, COP, the optimum electric current and thermoelement length.

Peter et al. [8] proposed a calculation procedure to define the optimum thermoelement length with the aim of maximizing cooling capacity and efficiency. Their model included the effect of the heat source temperature, heat sink temperature and the thermal resistance of the heat sink.

Another study on cooling capacity of the thermoelectric modules conducted by Yamanashi [9]. Yamanashi [9] investigated the optimum operation condition for a thermoelectric module to maximize COP. The author used a TEM with heat exchanger in the study.

Wang et al. [10] performed a study on COP of the TEMs. They concluded that the maximum COP values can be obtained by dividing the finite total thermal conductance into the hot side heat exchanger and the cold side heat exchanger.

Kishore et al. [11] investigated cooling performance of wearable thermoelectric coolers. The author stated that

external thermal resistance at hot side have great impacts on the TEM material behavior, design and performance of the TEM, and that these impacts are a fundamental challenge in achieving high efficiency for on-body applications. In their study, Kishore et al. [11] analyzed combined effect of heat source/sink thermal resistances and thermoelectric material properties on thermoelectric cooler performance.

TEMs have main advantages such as lightness, small size, silent and non-vibration working, easy to temperature control, no need working fluid like refrigerant, no requirement of maintenance [12]. On the other hand, TEMs are not widespread in cooling applications with high capacity due to their low cooling performance. Keeping the hot sides at a low temperature improves the cooling performance of TEMs. In this study, novel water and air coolers for the hot side of TEMs to be used in high-capacity cooling applications have been investigated. It is thus aimed to provide a contribution for the adaption of TEMs to applications with high cooling needs with high efficiency. For this purpose, different from the other studies in literature, TEM selections have been carried out for 300 W high cooling capacities. A cooling system with TEM designed for this cooling capacity has not been encountered in the literature. The selected TEMs have given rise to a high heat transfer dissipation rate at the hot side of the TEMs. The new heat sink-fan combinations, as well as novel water coolers, have been investigated for dissipation of the heat from the hot side of the TEMs. In the new heat sink-fan combinations, different air velocities, heat sink geometries and locations on TEMs have been discussed and heat sink dimension have been optimized. Direct contact and non-contact cooling water channels are designed for novel water cooler design. Vortex generators to increase heat transfer in direct contact designs have been examined. In non-contact designs, multi small diameter channels have been considered. The effect of material properties on TEM hot side temperature have also been discussed in non-contact designs.

2. Materials and Methods

2.1. Selection of TEMs

The TEMs, also called peltier modules, are semiconductor devices and they can generate a temperature difference between both sides because of the current supplied to them. As with all cooling devices, the Coefficient of Performance (COP) is the most important criteria when selecting a TEM. The COP can be written as Eqn. (2.1) for a TEM:

$$COP = \frac{\dot{Q}_c}{\dot{W}_e} \quad (2.1)$$

where \dot{Q}_c is the cooling capacity desired from TEM and \dot{W}_e is the required electrical work supplied to TEM in order to provide \dot{Q}_c .

The required electrical power is supplied to TEM via current in a certain voltage [17]. The input power is as follow

$$\dot{W}_e = V \times I \quad (2.2)$$

where V and I are voltage and current, respectively. According to Eqn. (2.2), it is obvious that the current and voltage of the TEM are important to maximize the COP of the TEM. On the other hand, they affect to cooling capacity of the TEM due to changing temperature differences between hot and cold sides of the TEM. Therefore, the definition of optimal current and voltage values that minimize input power plays a key role when choosing TEM for a cooling application. Other important parameters should be considered as the determination of hot side temperature and of the temperature difference between both side of the TEM.

In the current study, the selection of the TEM is carried out for $\dot{Q}_c = 300$ W cooling capacity. The hot-side temperature of the TEM is defined as 50°C to dissipate heat to ambient at 30°C . The temperature difference between the cold and hot side of the TEM is 50°C to create a cooling effect via low temperature. Two type TEM which are FPH1-19922S1 [14] and FPH1-12712AC [15] is selected for 300 W cooling capacity. It is considered to obtain 300 W cooling capacity by using FPH1-19922S1 and FPH1-12712AC modules together. The geometrical details of the selected modules are presented in Figure 1.

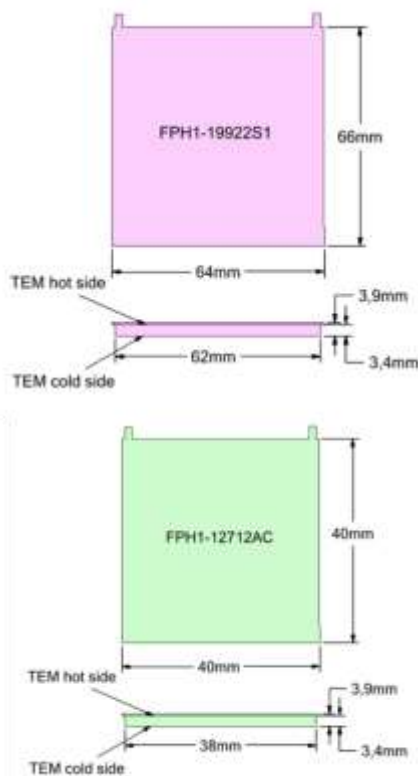


Figure 1. Geometrical details of (a) FPH1-19922S1 and, (b) FPH1-12712AC [14,15].

The performance curves of the selected FPH1-19922S1 and FPH1-12712AC modules are given in Figure 2. For the 50°C hot-side temperature, 22 A current is selected for operation of FPH1-19922S1 while 12.5 A is chosen for FPH1-12712AC. In this operation condition, the performance values of the selected TEMs are presented in Table 1. According to Table 1, two FPH1-19922S1 and one FPH1-12712AC are employed for $\dot{Q}_c = 300$ W cooling capacity.

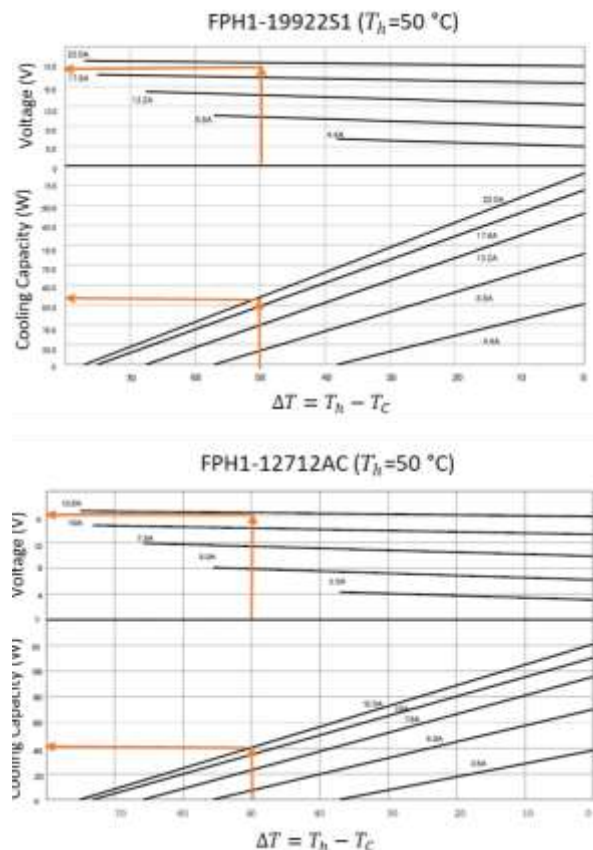


Figure 2. Performance curves of FPH1-19922S1 and FPH1-12712AC [14,15].

Table 1. The performance values of the selected TEMs.

	FPH1-19922S1	FPH1-12712AC
Voltage, V (volt)	25	16
Current, I (A)	22	12.5
Power, \dot{W}_e (W)	550	200
Cooling capacity, \dot{Q}_c (W)	130	40
COP (-)	0.236	0.2

TEM is a cooling device, and its energy interactions are given in Figure 3. in terms of the first law of thermodynamics. It can easily be observed in Figure 3 that heat dissipation from the hot side (\dot{Q}_h) of TEM is the sum of the cooling capacity and input power according to the first law of thermodynamics.

Thus, the heat dissipation rate from the hot side of TEM can be written as follow

$$\dot{Q}_h = \dot{Q}_c + \dot{W}_e \quad (2.3)$$

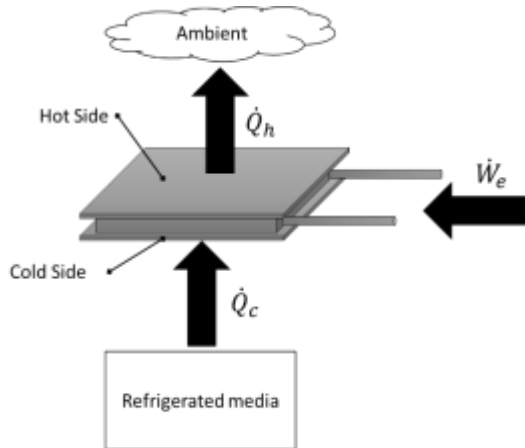


Figure 3. Energy interactions of a TEM.

The minimal total heat dissipation from the hot side decreases the input power of TEM for the constant cooling capacity. It is obvious that this situation improves the COP of the TEM. Hence, effective cooling of the hot side of TEM gains great importance for the applications. In the selected TEMs, FPH1-19922S1 has 680 W heat dissipation rates whereas FPH1-12712AC has 240 W.

2.2. Design of air-cooled for hot side of TEM

The removal of heat from the hot side of TEM at a high rate facilitates to reach the desired cooling capacity with low power. In other words, it increases COP. One of the ways of removing heat from the hot side is using a heat sink-fan combination. While the heat sink increases the heat transfer area, the fan creates forced convection between the fins of the heat sink.

In this study, 680 and 240 W heat should be dissipated from the hot sides of the selected TEMs to provide the desired cooling capacity. Designs of heat sink have been performed as an air-cooler for hot side of TEMs. The designs have been simulated, analyzed, and optimized by the HeatSinkCalculator [16] tool. For driving air between the designed heat sink fins, a high-capacity fan with a blade diameter of 120 mm and an airflow rates up to 271 CFM has been employed. The fan curve given in the Table 2 has been implemented in the

HeatSinkCalculator [16] tool. The placement of the heat sink-fan combination is given in Figure 4.

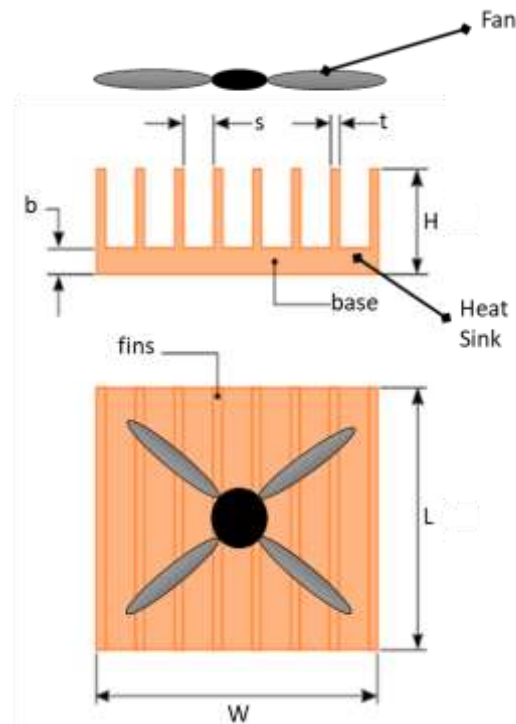


Figure 4. Front and top view of the heat sink-fan combination and dimensions of the heat sink.

Three heat sinks have been designed considering the dimensions of the fan and TEM. The designs are given in Figure 5. and they have been simulated and optimized using the HeatSinkCalculator [16]. The designs have been simulated for L values range between 63 and 120 mm, H values ranged from 20 to 70 mm and W values varied from 63 to 120 mm for FPH1-19922S1 TEM. Similarly, for FPH1-12712AC, L, H and W values have been changed in the designs at the ranges 63-100 mm, 20-60 mm and 63-120 mm, respectively. For these designs, the b, t, and s dimensions shown in Figure 4. have been optimized to minimize the source temperature (in other words, hot side temperature). It is worth to note here that the thermal resistance of the thermal paste has been considered in the simulations in the HeatSinkCalculator [16]. The thermal conductivity of the thermal paste has been assumed as 1.5 W/mK. Another assumption is that radiation in the heat sink is ignored.

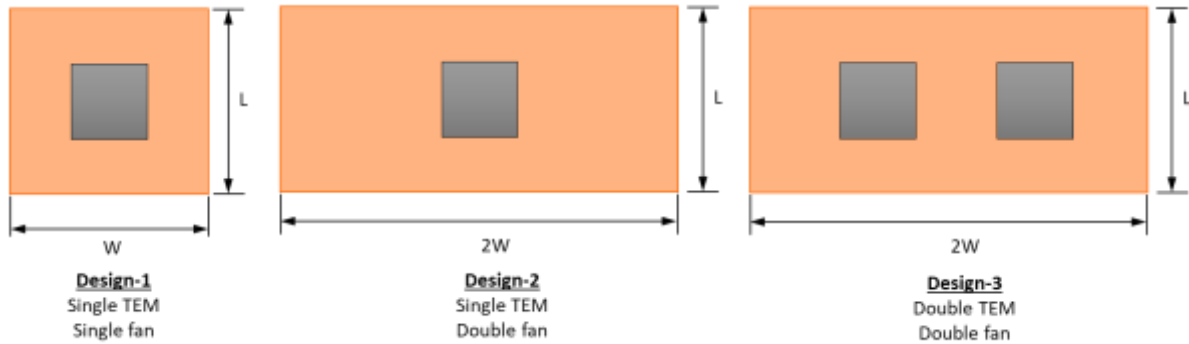


Figure 5. Simulated heat sink-fan system design for the investigated TEMs.

Table 2. Fan curve.

Air Volume (CFM)	Static Pressure (in-H ₂ O)
0	1.2
25	1.15
50	1.1
75	1
100	0.7
125	0.5
150	0.42
175	0.45
200	0.4
225	0.3
250	0.2

2.3. Design of water-cooled for hot-side of TEM

Considering its thermophysical properties, water is a better heat carrier than air. Water is a good cooler alternative for the high heat disposal that occurs on the hot side of TEMs depended upon the high cooling capacity. For this reason, two different water-cooling units, direct contact, and non-contact, are designed to cool the hot side of TEM. In direct contact design, the water at 35 °C used as the coolant is in direct contact with the hot side of the TEM. Direct contact design is presented in Figure 6. There is no solid wall between the water and the hot surface of the TEM. With this approach, the thermal resistance of the solid wall and thermal paste between the water and the hot surface is eliminated. Thus, it is aimed to increase the efficiency of heat transfer. In addition, by placing vortex generators in the channel, turbulent flow is created in the channel at low water inlet velocities. Thus, it is aimed to increase the heat transfer coefficient in regions close to the hot surface of TEM. Another advantage of direct contact design is that it can be manufactured from a polymer material. This situation provides both time and costs savings in terms of manufacturing. The width and length of the design has been determined based on the dimension of the TEM (Figure 1).

On the other hand, it is very difficult to seal in direct contact design. Therefore, the non-contact design has been realized to cool TEM hot side with water at 35 °C. The non-contact design and its dimensions are given in the Figure 7. In the non-contact design, channels with a small hydraulic diameter (6.667 mm) are used to regulate the flow and increase the heat transfer coefficient. The walls between the channels act as a fin and contribute to heat transfer. Although sealing is provided with this design, the solid wall and thermal paste between the hot surface and the water cause thermal resistance. This situation causes a slight decrease in the heat transfer rate. In order to reduce the thermal resistance, a design made of copper material with a higher thermal conductivity than aluminum is included in this study. However, it is worth to emphasize here that although the copper material decreases the thermal resistance, it increases the cost. The dimension of the design has been determined based on the TEM dimension (Figure 1). In this respect, the non-direct contact surface dimension has been applied as 63 mm × 63mm. According to total width and length, 5 × 10 mm channels have been designed (Figure 7). The one channel cross-sectional area is 50 mm².

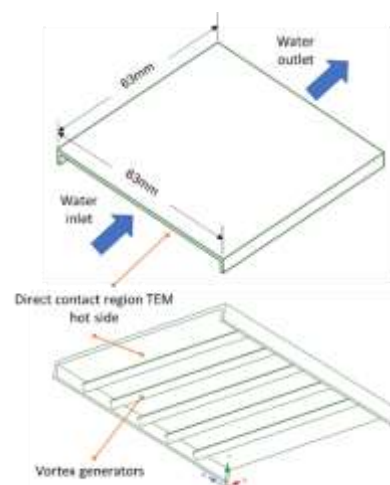


Figure 6. Direct contact design as a water-cooled unit.

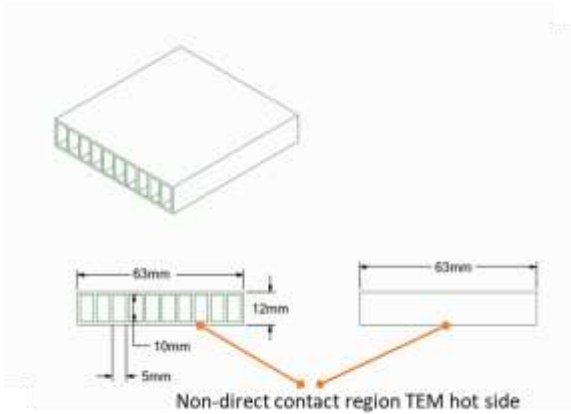


Figure 7. Non-direct contact design as a water-cooled unit.

2.3.1. Numerical Simulation of water-cooled designs

In this study, the direct contact and non-contact designs have been investigated numerically. A finite volume method has been used to solve the governing equations given in Eqns. (2.4) -(2.8) [13]. The governing equations (the mass, momentum, and energy conservation equations) for the steady incompressible flow, neglecting the viscous dissipation, are given as follows

$$\frac{\partial u}{\partial x} + \frac{\partial v}{\partial y} + \frac{\partial w}{\partial z} = 0 \quad (2.4)$$

$$\begin{aligned} \rho \left(u \frac{\partial u}{\partial x} + v \frac{\partial u}{\partial y} + w \frac{\partial u}{\partial z} \right) \\ = - \frac{\partial p}{\partial x} \\ + \mu \left(\frac{\partial^2 u}{\partial x^2} + \frac{\partial^2 v}{\partial y^2} + \frac{\partial^2 w}{\partial z^2} \right) \end{aligned} \quad (2.5)$$

$$\begin{aligned} \rho \left(u \frac{\partial v}{\partial x} + v \frac{\partial v}{\partial y} + w \frac{\partial v}{\partial z} \right) \\ = - \frac{\partial p}{\partial y} \\ + \mu \left(\frac{\partial^2 u}{\partial x^2} + \frac{\partial^2 v}{\partial y^2} + \frac{\partial^2 w}{\partial z^2} \right) \end{aligned} \quad (2.6)$$

$$\begin{aligned} \rho \left(u \frac{\partial w}{\partial x} + v \frac{\partial w}{\partial y} + w \frac{\partial w}{\partial z} \right) \\ = - \frac{\partial p}{\partial z} \\ + \mu \left(\frac{\partial^2 u}{\partial x^2} + \frac{\partial^2 v}{\partial y^2} + \frac{\partial^2 w}{\partial z^2} \right) \end{aligned} \quad (2.7)$$

$$\begin{aligned} \rho C_p \left(u \frac{\partial T}{\partial x} + v \frac{\partial T}{\partial y} + w \frac{\partial T}{\partial z} \right) \\ = k \left(\frac{\partial^2 T}{\partial x^2} + \frac{\partial^2 T}{\partial y^2} + \frac{\partial^2 T}{\partial z^2} \right) \end{aligned} \quad (2.8)$$

The numerical simulations have been performed with Ansys FLUENT R19.2 Academic Version [18]. Due to the geometrical difference of the designs, different computational domains have been considered for the direct contact and non-contact designs. The small-scale channels in the non-contact design are parametric. Therefore, one channel has been evaluated as a computational domain in the simulations to save computation time and effort. The direct contact design includes a channel with vortex generators, as seen in Figure 6. Thus, this channel has been used as the computational domain in the numerical simulation of the non-contact design. The small-scale channels in the non-contact design are parametric. Therefore, one channel has been considered as a computational domain in the simulations of non-contact designs to save computation time and effort. The computational domains of the designs are presented in Figure 8.

According to the Figure 6 and Figure 8, the hydraulic diameter of the water channel is 5.723 mm in direct contact design. Due to the vortex generator, there are very small cross-sections between walls and corners of vortex generators through the channel. These cross-sections have a 0.872 mm characteristic length. Considering this characteristic length, for $\dot{m}=200$ kg/h, Reynolds number is computed as 2729. The flow regime inside the channel is turbulent because of higher values of Reynolds number than 2300. In the non-contact design, the water flows in the channels with a 50 mm² cross-section. In addition, the channels have a 6.667mm hydraulic diameter. In this condition, Reynolds number is 1135 in a channel for $\dot{m}=200$ kg/h. Hence, the flow in the non-contact design is laminar.

As stated earlier, the heat dissipation rate from the hot site of TEM is 680 W for FPH1-19922S1 module. This heat rate should be removed from the 62 x 62 mm surface of the TEM. Therefore, heat flux at TEM hot surface has been calculated as 171.327 kW/m². In the numerical simulation, this heat flux has been applied as a boundary condition at direct contact and non-contact regions in the water-cooled designs.

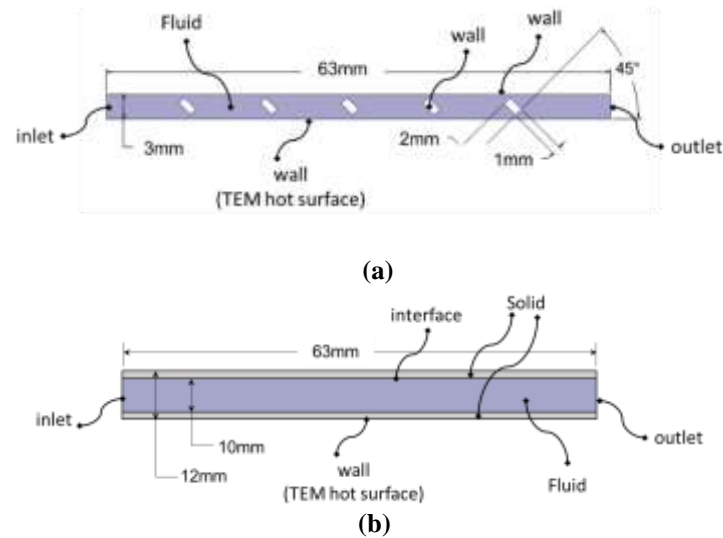


Figure 8. Computational domains (a) direct contact, (b) non-direct contact designs.

In the simulations, the flow has been numerically computed as 3D, turbulent, incompressible for direct contact design. The turbulent flow in direct contact design has been computed with standard k-epsilon. Similarly, 3D, laminar and incompressible flow has been simulated for non-contact design. In the numerical model, the convection terms have been discretized using the second-order upwind scheme while the diffusion terms are discretized using the central difference scheme. The SIMPLE algorithm has been used to couple the pressure and velocity. Convergence of the iterative solution has been insured when the residual of all the variables is less than the specified values. The specified convergence criteria are 10^{-3} for continuity, 10^{-5} for momentum, and 10^{-6} for energy. The computational domain of direct contact design consists of 312356 elements while there are 76882 rectangular elements in the computational domain of non-direct design. The mesh independence of the solution has been assured for both designs.

3. Results and Discussion

Table 3 shows heat sink optimized dimensions for both FPH1-19922S1 and FPH1-12712AC TEMs. Dimensions have been optimized to minimize the hot-side temperature of the TEMs. The dimensions H, L, and W have been optimized at the upper value of the optimization range in all considered designs of both TEMs. The basic dimensions H, L, and W have been as high as possible due to the high heat flux arising on the hot side of the TEMs. A similar situation is valid for the optimized dimensions b, t, and s. In all designs simulated for FPH1-19922S1 and FPH1-12712AC TEMs, the base thicknesses have been determined as the upper value of the optimization range (1-15 mm). Heat conduction resistance of metal materials is generally higher than heat convection resistance. With the maximum thickness of the base, the heat is transferred

over the heat sink by conduction in the longest possible way instead of convection. This allows heat to be expelled at a high rate from the hot side of the TEM thanks to lower thermal resistance in the heat sink. As one can observe from the Table 3, as a result of the optimization, the t and s values have been minimized; the number of fins has been increased. In this way, the heat transfer surface area has been increased. The heat transfer coefficient can be improved by increasing the heat transfer surface area. But it should not be forgotten that increasing the number of fins and decreasing the distance between them may cause a decrease in the air velocity between the fins of the heat sink. This situation can give rise to a decrease in the heat transfer coefficient at the airside. In the current study, this problem has been avoided by using a high-capacity fan, and a basis has been created for using as many fins as possible.

Fin efficiency, flow rate, and pressure drop of the air flowing over the fins of the heat sink are given in the Table 4. According to Table 4, Design-2 and Design-3 have the same fin efficiency in both TEMs due to their similar geometric features. The fin efficiencies of Design-2 and Design-3 are 0.74 in FPH1-19922S1 and are 0.78 in FPH1-12712AC. It is worth to mention here that the same fan is used in all simulations. The Design-1 simulated for TEMs has lower fin efficiency than Designs-2 and Designs-3. The main reason is that Design-1 causes lower air velocity and high-pressure drop between the fins. This situation decreases the heat transfer coefficient between the fins and, hence, decreases the fin efficiency.

Table 3. The optimized heat sink dimensions for both FPH1-19922S1 and FPH1-12712AC TEMs.

	FPH1-19922S1			FPH1-12712AC		
	Design-1	Design-2	Design-3	Design-1	Design-2	Design-3
H (mm)	70	70	70	60	60	60
L (mm)	120	120	120	100	100	100
W (mm)	120	240	240	120	240	240
b (mm)	14.5	15	15	15	15	15
t (mm)	1	1	1	1	1	1
s (mm)	1.25	1.3	1.32	1.2	1.13	1.13
N_f	54	105	104	55	113	113

Table 4. Fin efficiency, flow rate, and pressure drop of the air flowing over the fins of the heat sink designs.

	FPH1-19922S1			FPH1-12712AC		
	Design-1	Design-2	Design-3	Design-1	Design-2	Design-3
η_f	0.701	0.742	0.743	0.748	0.783	0.784
ν (m ³ /s)	0.0354	0.0531	0.0535	0.0307	0.0449	0.0448
Δp (Pa)	250	153	151	259	189	190

As mentioned earlier, FPH1-19922S1 and FPH1-12712AC as two different TEMs cause different hot side heat removal rates and COP values (Table 1). The heat to be removed from the hot-side of the FPH1-19922S1 TEM is 680 W at $\Delta T=50$ °C ($\Delta T=T_h - T_c$) while it is 240 W for FPH1-12712AC TEM. At these conditions, FPH1-19922S1 and FPH1-12712AC TEMs can provide 130 and 40 W cooling capacity, respectively. The thermal performances of the designs have been analyzed for these heat transfer rates. A comparison of the designs in terms of the highest temperature on the hot side of the modules and the lowest temperature on the cold side of the modules is presented in Table 5. According to Table 5, the maximum temperatures in the simulated designs for FPH1-19922S1 are 92.3 °C in Design-1, 89.4 °C in Design-2 and 98.9 °C in Design-3. Design-2 has been exhibited the lowest maximum temperature at the hot-side of the TEM. Unlike Design-2, Design-3 has been caused the highest hot side temperature with 98.9 °C for FPH1-19922S1. In Design-1, the maximum temperature has been determined as 92.3 °C. The

simulated temperature distributions for FPH1-19922S1 and FPH1-12712AC TEMs are given in Figure 9 and Figure 10, respectively. It can be seen from Figure 9 and Figure 10 that the highest temperature occurs at the midpoint of the modules. Accordingly Figure 9, doubling the width of the heat sink (Design-2) for the FPH1-19922S1 has been resulted in only a 3.142% reduction in maximum temperature. When Design-1 and Design-3 are examined, it is seen that using two TEMs separately with two narrow heat sinks instead of placing two TEMs in a single large heat sink results in lower maximum temperatures. Similar results can be observed in the FPH1-12712AC TEM with a lower heat rejection. According to Figure 10, the lowest maximum temperature for the hot side of the TEM has been exhibited by Design-2 with 64.3 °C. It is followed by Design-1 with 65.7 °C and Design-3 with 67.6 °C, respectively. For the FPH1-12712AC module, doubling the width of the heat sink (Design-2) instead of the single narrow heat sink (Design-1) has caused the maximum temperature on the hot side of the module to drop by only 2.13%.

Table 5. Maximum temperature at hot side of TEMs (T_h) and minimum temperature at cold side of the TEMs (T_c) for investigated heat sink-fan combinations.

	FPH1-19922S1 ($\dot{Q}_h=680$ W/ $COP=0.236$)			FPH1-12712AC ($\dot{Q}_h=240$ W/ $COP=0.2$)		
	Design-1	Design-2	Design-3	Design-1	Design-2	Design-3
T_h (°C)	92.3	89.4	98.9	65.7	64.3	67.6
T_c (°C)	42.3	39.4	48.9	15.7	14.3	17.6

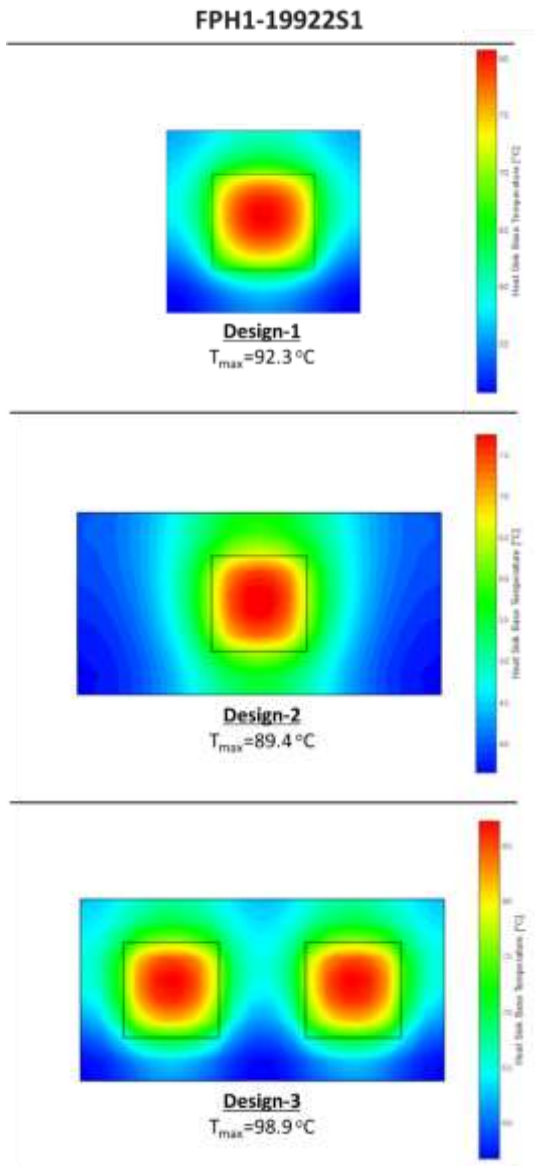


Figure 9. The simulated temperature distributions for FPH1-19922S1 TEM.

As explained before, the temperature difference between the cold and hot sides of the TEMs has been determined as 50 °C. The simulated lowest maximum temperature for the hot side of FPH1-19922S1TEM is 89.4 °C (Figure 9). In this case, the temperature of the cold side of the TEM is 39.4 °C. With its air-cooled heat sink designs, the FPH1-19922S1 module cannot create a cooling effect at 30 °C ambient temperature. In the FPH1-12712AC module, the simulated lowest maximum temperature for the hot side is 64.3 °C (Figure 10) and the lowest temperature for the cold side is 14.3 °C. This temperature value on the cold side of FPH1-12712AC has been reached with Design-2, and a close temperature can be obtained with Design-1. Accordingly, it is possible to provide a cooling effect in an environment at 30 °C with the FPH1-12712AC module.

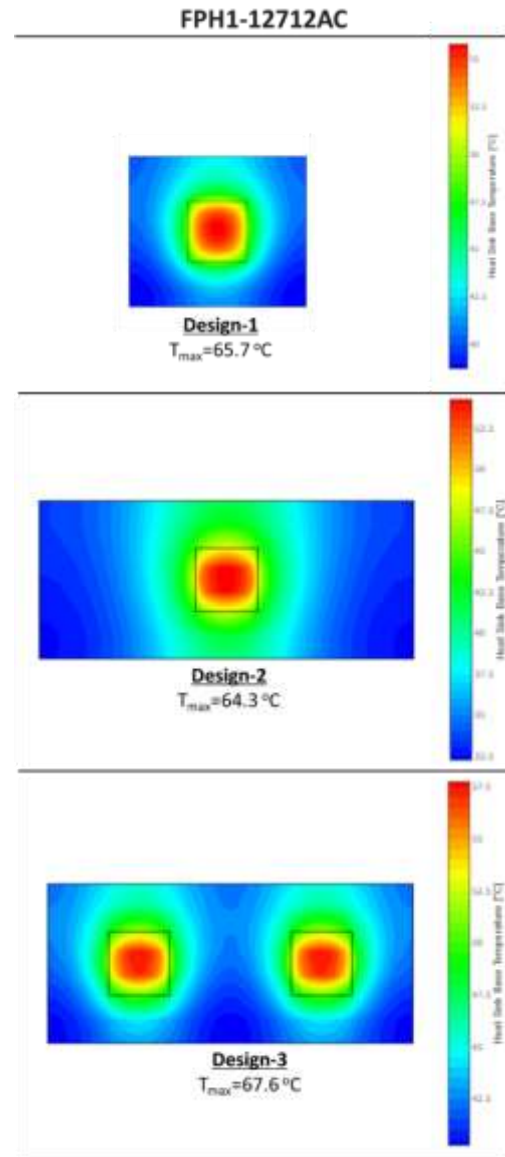


Figure 10. The simulated temperature distributions for FPH1-12712AC TEM.

For better performance, water-cooled designs have been considered as well as air-cooled designs. The temperature contour of the direct contact design is given in the Figure 11. According to the Figure 11, the highest temperature is 52.9 °C while the lowest temperature is 42.1 °C on the TEM hot surface. On the surfaces that coincide with the back of the vortex generator, it is seen that the temperature decreases 42 °C. The main reason of this decrease is that the vortex generators disrupt the flow pattern and create mixed flow (in other words flow with vortex). The mixed flow regions can be seen in Figure 12. In these mixed-flow regions, the heat transfer coefficient increases significantly and cools the surface. For this design, the simulated average temperature on the hot surface of TEM is 43.31 °C.

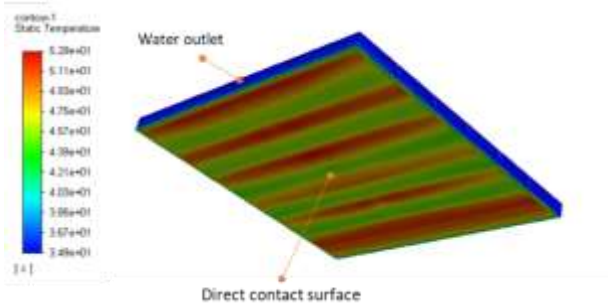


Figure 11. The temperature contour of the direct contact design.

In another water-cooled design, the effect of the material is also taken into account besides the channel geometry. The temperature distribution occurring in the non-direct design made of copper material is given in the Figure 13. The highest temperature occurring on the TEM hot surface is 75.9 °C. When the temperature is in the range of 50-55 °C in the regions corresponding to the entrance of the channel, the temperature increases towards the channel outlet. According to the temperature map given in the figure, water enters at 35 °C and leaves the channel at 41.4 °C. With the heat flux provided by TEM, there is an increase of 6.4 °C in the temperature of the cooling water. The heat transfer rate of the water, heated by heat flux provided by the TEM, has decreased along the channel due to the decrease of the finite temperature difference between the hot surface of TEM and water. This situation caused the TEM hot surface temperature to increase towards the channel outlet. The average temperature of the TEM hot surface has been simulated as 68.96 °C.

Similarly, the simulated temperature distribution of the non-contact design made of aluminum material is given in the Figure 14. A similar situation has been encountered with the copper material non-direct design. TEM hot surface temperature has increased towards the outlet due to the heating of the cooling water. According to the simulation results, the temperature average of the TEM hot surface is 75.22 °C in the aluminum non-direct design.

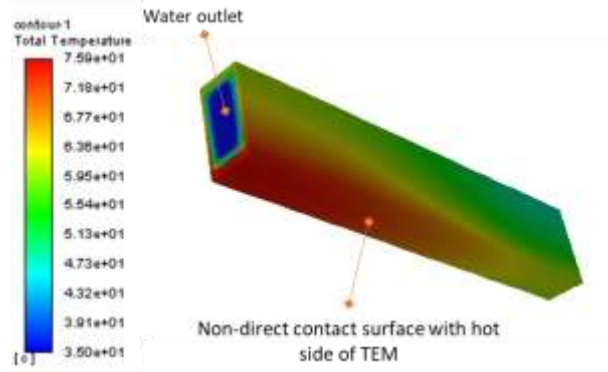


Figure 13. The temperature contour of the non-direct contact design made of copper.

By using aluminum instead of copper, the heat transfer coefficient of the solid wall is reduced by approximately 50%. This situation causes the average temperature of the TEM hot surface to increase by 6.26 °C (8.62%).

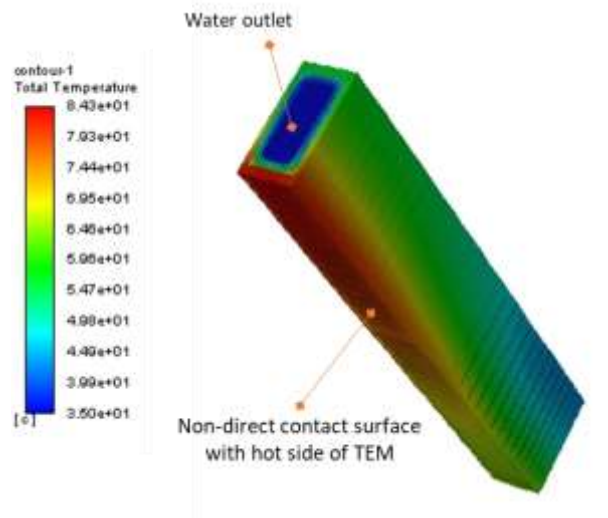


Figure 14. The temperature contour of the non-direct contact design made of copper.

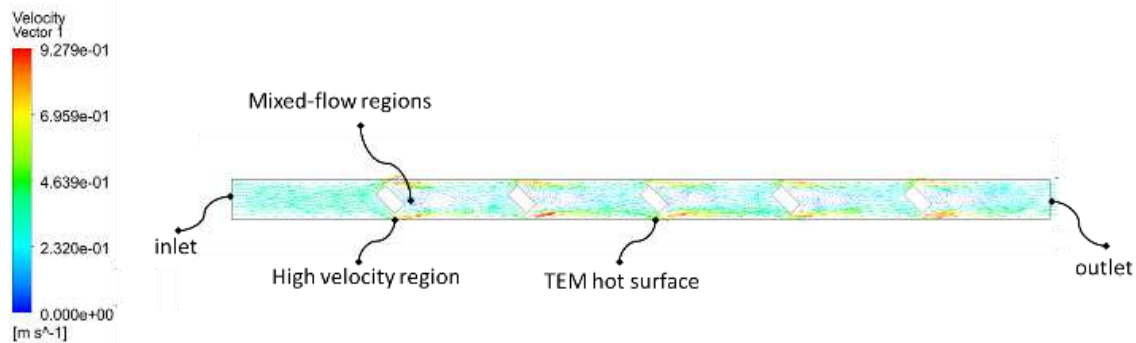


Figure 12. Representation of velocity vectors and mixed flow regions.

4. Conclusion

For cooling applications having TEM, the energy that must be dissipated from the hot side is always much higher than absorbed energy from the cold side of the TEM according to first law of thermodynamics (Eqn. (2.3)). Temperature difference between hot and cold side of the TEM is also a matter which must be considered because as the temperature difference increases, cooling capacity of the TEM decreases. Therefore, cooling of the hot side of the TEMs is crucial for the cooling applications. For cooling of hot side of the TEMs, a proper way can be found by using the heat sinks and fan combinations and water-cooling systems as shown in this study.

Accordingly air-cooled designs to cool the hot side of the TEM for 300 W refrigeration capacity, doubling the width of the heat sink (for one TEM) instead of the single narrow heat sink caused reductions in the maximum temperature at the hot side of the TEMs. But these reductions in the maximum temperature at the hot side of the TEMs were between 2-4%.

In this study, it is also observed that using two TEMs separately with two narrow heat sinks instead of placing two TEMs in a single large heat sink results in lower maximum temperatures at the hot side of TEMs.

It concluded that air-cooled system give rise to higher temperatures at the hot side of the TEM than water cooling system. In the water-cooling designs, elimination of thermal resistance of the solids between water and the hot side of the TEMs and creating turbulent flow via vortex generation improved cooling performance of the designs.

Acknowledgement

This research was supported by ISM Makine Elektrik Sanayi ve Ticaret A.Ş. We would like to thank our colleagues in the Ismart Department of ISM Makine Elektrik Sanayi ve Ticaret A.Ş., who helped the research with great expertise and enthusiasm.

Author's Contributions

Anil BAŞARAN: Drafted and wrote the manuscript, performed the energy analysis, numerical simulations and result analysis.

Uğur PEHLİVANOĞLU: Performed selection of TEMs and fan, assisted in analytical analysis on the structure, supervised the energy analysis, result interpretation and helped in manuscript preparation.

Ethics

There are no ethical issues after the publication of this manuscript.

*This study was presented at The III. National University-Industry Cooperation R&D and Innovation Congress.

References

1. Rowe, D.M. Application of thermoelectric cooling. In. CRC Handbook of Thermoelectrics, CRC Press Inc., Boca Raton, 1995, pp 617- 683.
2. Riffat, S.B., Omer, S.A. and Ma, X. 2001. A novel thermoelectric refrigeration system employing heat pipes and a phase change material: an experimental investigation. *Renewable Energy* 23, 313–323.
3. Venkatesan, K., Venkataramanan, M. 2020. Experimental and smulation studies on thermoelectric cooler: a performance study approach. *International Journal of Thermophysics* 41 (4), 1-23.
4. Ahıska, R. and Ahıska, K. 2007. Esnek iki fazlı termoelektrik CPU soğutucusu. *Gazi Üniv. Müh. Mim. Fak. Dergisi* 22 (2), 347-351.
5. Deniz, E.B., Kavak, B., Arslan, K. 2015. Seri Bağlı Ardışık Termoelektrik Soğutucuların Soğutma Performanslarının Deneysel İncelenmesi. *NWSA-Engineering Sciences*, 10.03.1A0357.
6. Jeong, E.S. 2014. A new approach to optimize thermoelectric cooling modules. *Cryogenic*, 59, 38-43.
7. Jeong, E.S. 2021. Optimization of thermoelectric modules for maximum cooling capacity. *Cryogenics* 114, 103241.
8. Pettes, A.M., Hodes, M.S., Goodson, K.E. 2009. Optimized thermoelectric refrigeration in the presence of thermal boundary resistance. *IEEE Trans Adv Pack* 32, 423-430.
9. Yamanashi, M. 1996. A new approach to optimum design in thermoelectric cooling systems. *Journal of Applied Physics* 80, 5494-5502.
10. Wang, X., Yu, J., Ma, M. 2013. Optimization of heat sink configuration for thermoelectric cooling system based on entropy generation analysis. *International Journal of Heat and Mass Transfer* 63, 361-365.
11. Kishore, R.A., Nozariasbmarz, A., Poudel, B., Sanghadasa, M. and Priya, S. 2019. Ultra-high performance wearable thermoelectric coolers with less materials. *Nature communications* 10 (1), 1-13.
12. Meng, J.H., Wu, H.C., Gao, D.Y., Kai, Z., Lu, G., Yan, W.M. 2021. A novel super-cooling enhancement method for a two-stage thermoelectric cooler using integrated triangular-square current pulses. *Energy* 217, 119360.
13. Çengel, Y.A., Boles, M.A., Kanoğlu, M. Thermodynamics: An Engineering Approach (9th Ed.), McGraw-Hill Education: NY, USA, 2018, pp:684.
14. Specification of FPH1-19922S1 TEM produced by Zmax Thermoelectric cooler and device manufacturer
15. Specification of FPH1-12712AC TEM produced by Zmax Thermoelectric cooler and device manufacturer.
16. Heat Sink Calculator Online Heat Sink Analysis and Design Tool. <https://www.heatsinkcalculator.com/> (accessed at 06.03.2021).
17. Versteeg, H.K. and Malalasekera, W. An introduction to computational fluid dynamics: the finite volume method. Pearson education: London, UK , 2007.
18. ANSYS® FLUENT, Release 19.2 Student Version